Transmission Grid Resiliency Investment Optimization Model With SOCP Recovery Planning

Kaitlyn Garifi, *Member, IEEE*, Emma S. Johnson, Bryan Arguello, *Member, IEEE*, and Brian J. Pierre, *Senior Member, IEEE*

***Abstract*—In the face of increasing natural disasters and an aging grid, utilities need to optimally choose investments to the existing infrastructure to promote resiliency. This paper presents a new investment decision optimization model to minimize unserved load over the recovery time and improve grid resilience to extreme weather event scenarios. Our optimization model includes a network power flow model which decides generator status and generator dispatch, optimal transmission switching (OTS) during the multi-time period recovery process, and an investment decision model subject to a given budget. Investment decisions include the hardening of transmission lines, generators, and substations. Our model uses a second order cone programming (SOCP) relaxation of the AC power flow model and is compared to the classic DC power flow approximation. A case study is provided on the 73-bus RTS-GMLC test system for various investment budgets and multiple hurricane scenarios to highlight the difference in optimal investment decisions between the SOCP model and the DC model, and demonstrate the advantages of OTS in resiliency settings. Results indicate that the network models yield different optimal investments, unit commitment, and OTS decisions, and an AC feasibility study indicates our SOCP resiliency model is more accurate than the DC model.**

***Index Terms*—Power system resilience, optimal transmission switching, investment decisions, mixed integer conic programming, power systems, power system planning, power system optimization.**

NOMENCLATURE

Sets

$\mathcal{L}$	Set of transmission lines $l = (i, j)$.
$\mathcal{L}_b^{\text{to}}$	Set of lines to bus b.
$\mathcal{L}_b^{\text{fr}}$	Set of lines from bus b.
$\mathcal{L}^{t,s}$	Set of lines impacted in scenario s at time t.
$\mathcal{B}$	Set of buses b.
$\mathcal{B}^{t,s}$	Set of buses b impacted in scenario s at time t.
$\mathcal{G}$	Set of generators g.
$\mathcal{G}_b$	Set of generators g at bus b.
$\mathcal{G}^{t,s}$	Set of generators impacted in scenario s at time t.
$\mathcal{R}$	Set of renewable energy sources (RES) r.
$\mathcal{R}_b$	Set of RES r at bus b.
$\mathcal{R}^{t,s}$	Set of RES impacted in scenario s at time t.

Parameters

$p_{\text{L},b}^t$	Real power load at bus b at time t.
$q_{\text{L},b}^t$	Reactive power load at bus b at time t.
i	Origin bus of line l.
j	Destination bus of line l.
B_l	Susceptance of line l.
G_l	Conductance of line l.
B_l^{ch}	Charging susceptance of line l.
B_b^{fs}	Fixed shunt susceptance at bus b.
G_b^{fs}	Fixed shunt conductance at bus b.
τ_l	Transformer tap ratio of transformer l.
$\bar{S}_l$	Short term thermal limit of line l.
RU_g	Ramp up limit of generator g.
RD_g	Ramp down limit of generator g.
$\underline{P}_g$	Minimum real power output of generator g.
$\overline{P}_g$	Maximum real power output of generator g.
$\underline{Q}_g$	Minimum reactive power output of generator g.
$\overline{Q}_g$	Maximum reactive power output of generator g.
$\underline{V}_b$	Minimum voltage magnitude at bus b (p.u.).
$\overline{V}_b$	Maximum voltage magnitude at bus b (p.u.).
$\underline{R}_r$	Lower curtailment limit of renewable source r.
$\overline{R}_r$	Upper curtailment limit of renewable source r.
p_r	Available generation from renewable source r.
C_l	Cost of hardening line l.
C_b	Cost of hardening bus b.
C_g	Cost of hardening generator g.
K	Investment budget.
β_b	Weight for criticality of load at bus b.

Variables

Common to both models

$p_{\text{S},b}^t$	Real power load shed at bus b at time t.
p_g^t	Real power output of generator g at time t.
$p_{\text{c},r}^t$	Curtailment of renewable source r.
x_l^t	Binary indicating switching status of line l at time t.

Manuscript received June 29, 2020; revised November 10, 2020 and April 5, 2021; accepted June 13, 2021. Date of publication July 1, 2021; date of current version December 23, 2021. This work was supported in part by the Department of Energy, Office of Electricity Delivery, and Energy Reliability, Advanced Grid Modeling Program led by Dr. Ali Ghassemian and in part by Sandia National Laboratories is a multimission laboratory managed, and operated by the National Technology and Engineering Solutions of Sandia, LLC, a wholly owned subsidiary of Honeywell International, Inc., for the U.S. Department of Energy's National Nuclear Security Administration under Contract DE-NA0003525. Paper no. TPWRS-01081-2020. *(Corresponding author: Kaitlyn Garifi.)*

Kaitlyn Garifi is with Sandia National Laboratories, Albuquerque, NM 87123 USA, and also with Lineage Logistics, San Fransisco, CA 94133 USA (e-mail: kgarifi@lineagelogistics.com).

Emma S. Johnson, Bryan Arguello, and Brian J. Pierre are with Sandia National Laboratories, Albuquerque, NM 87123 USA (e-mail: esjohn@sandia.gov; barguel@sandia.gov; bjpierr@sandia.gov).

Color versions of one or more figures in this article are available at https://doi.org/10.1109/TPWRS.2021.3091538.

Digital Object Identifier 10.1109/TPWRS.2021.3091538

z_l Binary indicating hardening decision for line l.
z_b Binary indicating hardening decision for bus b.
z_g Binary indicating hardening decision for generator g.
u_g^t Binary indicating status of generator g at time t.

SOCP Relaxation

$q_{\mathrm{S},b}^t$ Reactive power load shed at bus b at time t.
$p_{l,i}^t$ Real power flow on line l at time t from bus i.
$q_{l,i}^t$ Reactive power flow on line l at time t from bus i.
$p_{l,j}^t$ Real power flow on line l at time t to bus j.
$q_{l,j}^t$ Reactive power flow on line l at time t to bus j.
q_g^t Reactive power output at generator g at time t.

DC OPF

θ_b^t Voltage angle at bus b at time t.
p_l^t Power flow through line l at time t.

Notes: We will use the term lines to mean both lines and transformers (which are modeled as a line). Thus, for lines that are not transformers $\tau_l = 1$. Additionally, notation not included in this section will be introduced in the text.

I. Introduction

BOTH aging infrastructure and the increasing frequency of weather-caused electrical grid outages threaten the resilience of our grid. In the United States, over 70% of the transmission lines and transformers are over 25 years old, making them vulnerable to damage by weather, equipment failure, overgrown surrounding vegetation, and wildlife [1]. Severe weather is the most common cause of outage. In particular, there were 178 weather or climate disasters in the United States from 1980 to 2014, with 7 of the 10 costliest weather events occurring in the last 10 years of that period [2]. With the electrification of most daily tasks and critical services (such as hospitals and water treatment plants), resilience of the power grid is a top concern [2]. The authors of [3] argue that there is a need for a connection between outage scenario modeling and optimal grid investment selection for resilience.

To address this, we propose a model for choosing optimal investments in the existing transmission grid infrastructure to strengthen the resiliency of the system to weather-related scenarios, minimizing weighted unserved load in the network. The possible investments considered are hardening transmission lines, substations, and generators, which could include the selective undergrounding of transmission lines that serve critical infrastructure such as hospitals, elevating substations and building flood walls in areas susceptible to flooding, and investing in equipment and material stockpiles for outage response [4]. Our resiliency investment model uses both optimal transmission switching (OTS) and the second order cone programming (SOCP) relaxation of the AC optimal power flow (OPF) model for the network. This means the model captures both real and reactive power flows, and voltages. We compare the optimal resiliency investments to those obtained when the model uses a linear power flow approximation (DC OPF), as in [5], [6]. Additionally, we provide results justifying OTS in a resiliency setting and perform an AC feasibility study to demonstrate the optimal investment, unit commitment, and OTS decisions with the relaxed SOCP model are far more accurate compared to the linear DC model.

A. Literature Review

Various investment optimization models have been proposed for weather-driven resiliency of the transmission grid, however not all of these consider a time-indexed recovery model or a wide range of possible investments. Several models decide investments based on the system's initial response to a disaster rather than planning recovery over a time horizon. The authors in [7] use a stochastic model with a single-period convex relaxation of AC power flow to determine the cost-optimal investments in both new grid components and hardening of existing infrastructure. They motivate resiliency by ensuring a pre-specified fraction of the demand is met. The authors in [8] also seek to minimize the cost of investments, in this case line hardening decisions, in a transmission system with stochastic power flows due to a high penetration of renewable energy sources while satisfying the $N - k$ security criterion.

Several models have been proposed which include a time-indexed recovery model. A general framework for critical infrastructure recovery in a resilience context is discussed in [9]. They introduce a robust model to decide expansion and hardening for a network which plans recovery to disruptions, minimizing the total disruption over time. A model focused on only one type of investment, i.e., which generators should be converted to have black-start capabilities, is presented in [10]. They include unit commitment but not OTS in the recovery model. Although it is not an investment model, [11] is a pre-hurricane restoration model which also includes unit commitment in a recovery model over a time horizon. Several resiliency investment models taking into account recovery have also been proposed for the distribution grid [12]–[14].

Several works have considered including transmission switching as a disaster recovery strategy. Though they are not interested in resiliency investments, the authors in [15] consider both preventative and emergency response to natural disaster scenarios. Their models decide generator dispatch, topology switching, and, in the emergency response case, load shedding. The authors in [16] suggest co-optimizing transmission line switching and generator redispatch during the recovery stage to minimize load shed following an extreme weather event. Demand response strategies for large industrial customers have also been suggested to aid transmission grid resiliency in [17], where an SOCP relaxation with OTS is used from [18].

It has already been suggested that the DC power flow model is not an accurate enough relaxation in a resiliency context. A framework to optimally restore a transmission system while considering the co-optimization of repairs, load pickups, and generation dispatch in order to minimize load shed has been proposed in [19]. The authors find using a linear programming relaxation of AC power flow can often find restoration plans which can be made AC-feasible, whereas DC OPF does not. This work leverages the results in [20] that compare resilient

grid design and planning solutions for a DC power flow approximation, as well as a relaxed AC OPF model. We build on this work by adding OTS and generator status to the recovery model, expanding the possible investment options, and improving scenario complexity with time-indexed extreme weather events.

B. Contributions

In this work, we compare the optimal resilience investment results with two different power flow models: a DC approximation and an SOCP relaxation. We evaluate the different investment outcomes with respect to the initial extreme weather event impact, load shed over the recovery phase, total unserved energy, and the proportion of investment budget that is spent on different components. We also demonstrate the advantages of OTS in a resiliency setting, trade-offs between the investment budget limit and unserved load, and compare the AC feasibility of the resiliency outcomes with an SOCP relaxation versus a DC power flow model. Our main contributions are:

- We present an investment optimization model to improve grid resilience using a SOCP network model to model recovery during an extreme weather event. The recovery model also includes optimal transmission line switching, unit commitment, and generator dispatch over a multi-time period restoration horizon. The extreme weather event is modeled to account for components being impacted sequentially for the duration of the extreme weather scenario.
- We demonstrate that the optimal investment decisions obtained when considering a resiliency framework with the DC power flow approximation can vary from those obtained when the SOCP relaxation of the AC power flow model is used. We provide results that highlight trade-offs in the optimal investments with respect to the type of component as the investment budget varies. Furthermore, we show that the DC power flow model overestimates the benefit of the investments on reducing load shed.
- We show that including an OTS model in our resiliency framework mitigates some of the initial impact of the extreme weather event, and also aids in reducing unserved load during the later stages of the recovery phase. Further, our AC feasibility study shows that the optimal investments, together with the optimal unit commitment and OTS decisions, obtained with the SOCP relaxation are more accurate and closer to the load shed resiliency outcome than the DC model.

The rest of this paper is organized as follows: in Section II we first introduce the resiliency investment model with the network power flow constraints modeled with the SOCP relaxation. We then introduce the equivalent model with the DC OPF equations used to model the network power flow. In Section III, we provide a case study on the RTS-GMLC test system comparing the optimal investment decisions obtained under both models. In Section IV, we discuss the impact of the network model on the optimal solutions, as well as provide areas of future work.

II. Resiliency Investment Formulation

In this section, we present our resiliency investment model formulation that uses the SOCP relaxation of the AC power flow model and OTS, and includes generator ramping, a generator status model which includes physical but not economic constraints on the generators, and an investment budget limit. Then, a second formulation is introduced which uses the DC power flow approximation.

A. Formulation With SOCP Relaxed AC Power Flow Model

First, we formulate the resiliency investment model where power flows in the network are described using the SOCP relaxation of the AC power flow equations with transmission line switching [18]. A detailed description of the formulation is provided after the optimization problem. Our mixed-integer SOC problem (MISOCP), denoted $(\mathcal{P}_{soc})$, is given by:

$$(\mathcal{P}_{soc}) \quad \min \sum_{t\in\mathcal{T}}\sum_{b\in\mathcal{B}} \beta_b p^t_{\mathrm{S},b} \tag{1}$$

subject to:

$$\sum_{b\in\mathcal{B}} C_b z_b + \sum_{g\in\mathcal{G}} C_g z_g + \sum_{l\in\mathcal{L}} C_l z_l \le K \tag{2}$$

$$p^t_g - p^{t-1}_g \le RU_g, \qquad \forall g\in\mathcal{G}, \forall t\in\mathcal{T} \tag{3}$$

$$p^{t-1}_g - p^t_g \le RD_g u^t_g + \overline{P}_g(1-u^t_g), \quad \forall g\in\mathcal{G}, \forall t\in\mathcal{T} \tag{4}$$

$$\underline{P}_g u^t_g \le p^t_g \le \overline{P}_g u^t_g, \qquad \forall g\in\mathcal{G}, \forall t\in\mathcal{T} \tag{5}$$

$$\underline{Q}_g u^t_g \le q^t_g \le \overline{Q}_g u^t_g, \qquad \forall g\in\mathcal{G}, \forall t\in\mathcal{T} \tag{6}$$

$$\underline{V}^2_b \le c^t_b \le \overline{V}^2_b, \qquad \forall b\in\mathcal{B}, \forall t\in\mathcal{T} \tag{7}$$

$$p^t_{l,i} = x^t_l\left[c^t_i\frac{G_l}{\tau_l^2} + \left(\frac{-G_l}{\tau_l}c^t_{ij} - \frac{B_l}{\tau_l}s^t_{ij}\right)\right], \quad \forall l\in\mathcal{L}, \forall t\in\mathcal{T} \tag{8}$$

$$q^t_{l,i} = x^t_l\left[-\frac{1}{\tau_l^2}c^t_i\left(B_l + \frac{B^{\mathrm{ch}}_l}{2}\right) + \left(\frac{B_l}{\tau_l}c^t_{ij} - \frac{G_l}{\tau_l}s^t_{ij}\right)\right], \quad \forall l\in\mathcal{L}, \forall t\in\mathcal{T} \tag{9}$$

$$p^t_{l,j} = x^t_l\left[c^t_j G_l + \left(-\frac{G_l}{\tau_l}c^t_{ji} - \frac{B_l}{\tau_l}s^t_{ji}\right)\right], \forall l\in\mathcal{L}, \forall t\in\mathcal{T} \tag{10}$$

$$q^t_{l,j} = x^t_l\left[-c^t_j\left(B_l + \frac{B^{\mathrm{ch}}_l}{2}\right) + \left(\frac{B_l}{\tau_l}c^t_{ji} - \frac{G_l}{\tau_l}s^t_{ji}\right)\right], \quad \forall l\in\mathcal{L}, \forall t\in\mathcal{T} \tag{11}$$

$$(c^t_{ij})^2 + (s^t_{ij})^2 \le x^t_l\left[c^t_i c^t_j\right], \qquad \forall l\in\mathcal{L}, \forall t\in\mathcal{T} \tag{12}$$

$$c^t_{ij} = c^t_{ji},\ s^t_{ij} = -s^t_{ji}, \qquad \forall l\in\mathcal{L}, \forall t\in\mathcal{T} \tag{13}$$

$$(p^t_{l,j})^2 + (q^t_{l,j})^2 \le \bar{S}^2_l, \qquad \forall l\in\mathcal{L}, \forall t\in\mathcal{T} \tag{14}$$

$$(p^t_{l,i})^2 + (q^t_{l,i})^2 \le \bar{S}^2_l, \qquad \forall l\in\mathcal{L}, \forall t\in\mathcal{T} \tag{15}$$

$$\underline{R}_r \le p^t_{\mathrm{c},r} \le \overline{R}_r, \qquad \forall r\in\mathcal{R}, \forall t\in\mathcal{T} \tag{16}$$

$$\sum_{g\in\mathcal{G}_b} p^t_g - G^{\mathrm{fs}}_b c^t_b - \sum_{l\in\mathcal{L}^{\mathrm{to}}_b} p^t_{l,j} - \sum_{l\in\mathcal{L}^{\mathrm{fr}}_b} p^t_{l,i} + \sum_{r\in\mathcal{R}_b}(p^t_r - p^t_{\mathrm{c},r}) = p^t_{\mathrm{L},b} - p^t_{\mathrm{S},b}, \ \forall b\in\mathcal{B}, \forall t\in\mathcal{T} \tag{17}$$

$$\sum_{g\in\mathcal{G}_b} q_g^t + B_b^{\mathrm{fs}} c_b^t - \sum_{l\in\mathcal{L}_b^{\mathrm{to}}} q_{l,j}^t - \sum_{l\in\mathcal{L}_b^{\mathrm{fr}}} q_{l,i}^t = q_{\mathrm{L},b}^t - q_{\mathrm{S},b}^t, \quad \forall b\in\mathcal{B},\forall t\in\mathcal{T} \quad (18)$$

$$0 \le p_{\mathrm{S},b}^t \le p_{\mathrm{L},b}^t, \quad \forall b\in\mathcal{B},\forall t\in\mathcal{T} \quad (19)$$

$$0 \le q_{\mathrm{S},b}^t \le q_{\mathrm{L},b}^t, \quad \forall b\in\mathcal{B},\forall t\in\mathcal{T} \quad (20)$$

$$q_{\mathrm{S},b}^t = \frac{q_{\mathrm{L},b}^t}{p_{\mathrm{L},b}^t} p_{\mathrm{S},b}^t, \quad \forall b\in\mathcal{B},\forall t\in\mathcal{T} \quad (21)$$

$$x_l^t \le z_l \quad \forall l\in\mathcal{L}^{t,s},\forall t\in\mathcal{T} \quad (22)$$

$$u_g^t \le z_g \quad \forall g\in\mathcal{G}^{t,s},\forall t\in\mathcal{T} \quad (23)$$

$$u_g^t \le z_b \quad \forall b\in\mathcal{B}^{t,s},\forall g\in\mathcal{G}_b,\forall t\in\mathcal{T} \quad (24)$$

$$x_l^t \le z_b \quad \forall b\in\mathcal{B}^{t,s},\forall l\in\mathcal{L}_b^{\mathrm{to}},\forall l\in\mathcal{L}_b^{\mathrm{fr}},\forall t\in\mathcal{T} \quad (25)$$

for extreme weather event scenario s. The objective in (1) is to minimize total unserved load over the recovery horizon weighted according to criticality β_b. The total investment budget for lines, generators, and buses is given in (2). Generator ramp up and ramp down constraints for real power dispatch are given in (3)-(4). Note that RU_g and RD_g are physical ramping limits on the generators, not economic ones as in traditional unit commitment models. In addition, the ramp down constraint in (4) is modified to allow generators to trip off in an emergency without respecting ramping limits. Real and reactive generator dispatch limits are given in (5) and (6), respectively. Voltage limits are given in (7) and the thermal line limits are given in (14)-(15). In this work, all renewable sources are assumed to be fully curtailable, with curtailment limits enforced in (16). The SOCP relaxation of the AC OPF constraints with transmission line switching are given in (8)-(12). Note that the SOCP relaxation variables c_b^t for all $b\in\mathcal{B}$ and $t\in\mathcal{T}$, and $s_{ij}^t, s_{ji}^t, c_{ij}^t, c_{ji}^t$ for all $l\in\mathcal{L}$ and $t\in\mathcal{T}$ are additional decision variables added to the optimization. We reformulate the SOCP relaxed AC power flow constraints with OTS as in [18] by replacing (8)-(12) with:

$$p_{l,i}^t = c_{l|i}^t \tfrac{G_l}{\tau_l^2} + \left(\tfrac{-G_l}{\tau_l} c_{ij}^t - \tfrac{B_l}{\tau_l} s_{ij}^t\right), \quad \forall l\in\mathcal{L},\forall t\in\mathcal{T} \quad (26)$$

$$q_{l,i}^t = -\tfrac{1}{\tau_l^2} c_{l|i}^t \left(B_l + \tfrac{B_l^{\mathrm{ch}}}{2}\right) + \left(\tfrac{B_l}{\tau_l} c_{ij}^t - \tfrac{G_l}{\tau_l} s_{ij}^t\right), \quad \forall l\in\mathcal{L},\forall t\in\mathcal{T} \quad (27)$$

$$p_{l,j}^t = c_{l|j}^t G_l + \left(-\tfrac{G_l}{\tau_l} c_{ji}^t - \tfrac{B_l}{\tau_l} s_{ji}^t\right), \quad \forall l\in\mathcal{L},\forall t\in\mathcal{T} \quad (28)$$

$$q_{l,j}^t = -c_{l|j}^t \left(B_l + \tfrac{B_l^{\mathrm{ch}}}{2}\right) + \left(\tfrac{B_l}{\tau_l} c_{ji}^t - \tfrac{G_l}{\tau_l} s_{ji}^t\right), \forall l\in\mathcal{L},\forall t\in\mathcal{T} \quad (29)$$

$$x_l^t \underline{c}_{ij} \le c_{ij}^t \le x_l^t \overline{c}_{ij}, \quad \forall l\in\mathcal{L},\forall t\in\mathcal{T} \quad (30)$$

$$x_l^t \underline{s}_{ij} \le s_{ij}^t \le x_l^t \overline{s}_{ij}, \quad \forall l\in\mathcal{L},\forall t\in\mathcal{T} \quad (31)$$

$$x_l^t \underline{V}_j^2 \le c_{l|j}^t \le x_l^t \overline{V}_j^2, \quad \forall l\in\mathcal{L},\forall t\in\mathcal{T} \quad (32)$$

$$x_l^t \underline{V}_i^2 \le c_{l|i}^t \le x_l^t \overline{V}_i^2, \quad \forall l\in\mathcal{L},\forall t\in\mathcal{T} \quad (33)$$

$$c_i^t - \overline{V}_i^2(1-x_l^t) \le c_{l|i}^t \le c_i^t - \underline{V}_i^2(1-x_l^t), \ \forall l\in\mathcal{L},\forall t\in\mathcal{T} \quad (34)$$

$$c_j^t - \overline{V}_j^2(1-x_l^t) \le c_{l|j}^t \le c_j^t - \underline{V}_j^2(1-x_l^t), \ \forall l\in\mathcal{L},\forall t\in\mathcal{T} \quad (35)$$

$$(c_{ij}^t)^2 + (s_{ij}^t)^2 \le c_{l|i}^t c_{l|j}^t, \quad \forall l\in\mathcal{L},\forall t\in\mathcal{T} \quad (36)$$

where new variables $c_{l|i}^t = c_i^t x_l^t$ and $c_{l|j}^t = c_j^t x_l^t$ are introduced for the bilinear terms. The line power flow constraints in (26)-(29), along with (30)-(33), ensure that the power flows and voltages take the correct value when the line is switched on and zero otherwise. The constraints in (34) and (35) are the McCormick relaxations of $c_{l|i}^t = c_i^t x_l^t$ and $c_{l|j}^t = c_j^t x_l^t$, respectively. The constraint in (36) replaces (12) with the new variables $c_{l|i}^t$ and $c_{l|j}^t$. The real and reactive power balance at each bus is given in (17) and (18), respectively. The limits on load shed are given in (19)-(21) which ensure load shed cannot exceed demand, and reactive power load shed is proportional to real power load shed. Lastly, the constraints in (22)-(25) ensure that the status variables for components (generators, buses, and lines) are coupled with investment decisions, i.e., a component cannot be "on" unless it is invested in. Note the investment constraints do not constrain x_l^t or u_g^t when they are invested in or not impacted by the extreme weather event, which allows lines to participate in OTS and generators to be turned on and off.

B. DC OPF Network Model

Next, for the purpose of comparison, we provide the model where power flows in the network are described using the DC OPF equations with transmission line switching, similar to [5]. The overall mixed-integer linear program (MILP), denoted $(\mathcal{P}_{dc})$, is given by:

$$(\mathcal{P}_{dc}) \quad \min \ \sum_{t\in\mathcal{T}}\sum_{b\in\mathcal{B}} \beta_b p_{\mathrm{S},b}^t \quad (37)$$

subject to:

$$(2)-(5),(16),(19),(22)-(25),$$

$$-\tfrac{\pi}{3} \le \theta_b^t \le \tfrac{\pi}{3}, \quad \forall b\in\mathcal{B},\forall t\in\mathcal{T}, \quad (38)$$

$$p_l^t = x_l^t B_l(\theta_j^t - \theta_i^t), \quad \forall l\in\mathcal{L},\forall t\in\mathcal{T}, \quad (39)$$

$$-S_l x_l^t \le p_l^t \le S_l x_l^t, \quad \forall l\in\mathcal{L},\forall t\in\mathcal{T}, \quad (40)$$

$$\sum_{g\in\mathcal{G}_b} p_g^t - G_b^{\mathrm{fs}} - \sum_{l\in\mathcal{L}_b^{\mathrm{to}}} p_l^t - \sum_{l\in\mathcal{L}_b^{\mathrm{fr}}} p_l^t + \sum_{r\in\mathcal{R}_b} (p_r^t - p_{\mathrm{c},r}^t) = p_{\mathrm{L},b}^t - p_{\mathrm{S},b}^t, \ \forall b\in\mathcal{B},\forall t\in\mathcal{T}, \quad (41)$$

for extreme weather event scenario s. Notice the objective in $(\mathcal{P}_{dc})$ is identical to that in $(\mathcal{P}_{soc})$. The constraints in (38)-(40) are the DC OPF equations which describe power flows in the network. Lastly, the active power balance is given in (41). We linearize (39) with a McCormick relaxation by replacing (39) with:

$$B_l(\theta_j^t - \theta_i^t) - 2\pi B_l(1-x_l^t) \le p_l^t, \quad \forall l\in\mathcal{L},\forall t\in\mathcal{T} \quad (42)$$

$$p_l^t \leq B_l(\theta_j^t - \theta_i^t) + 2\pi B_l(1 - x_l^t), \quad \forall l \in \mathcal{L}, \forall t \in \mathcal{T}. \quad (43)$$

Using the two resiliency investment formulations given in $(\mathcal{P}_{soc})$ and $(\mathcal{P}_{dc})$, we compare the impact of the network power flow model on the optimal resiliency investment decisions, as well as total load shed and recovery. Additionally, notice that both $(\mathcal{P}_{soc})$ and $(\mathcal{P}_{dc})$ include an OTS model and a unit commitment model by not requiring $x_l^t = 1$ and $u_g^t = 1$, respectively.

III. Resiliency Investment Case Study

We compare the proposed resiliency investment models given in $(\mathcal{P}_{soc})$ and $(\mathcal{P}_{dc})$ on the RTS GMLC test system [21] for improved resiliency to hurricane scenarios. The optimal investment decisions are compared for various fixed investment budgets on each of three different hurricane scenarios. The resiliency investment formulations in $(\mathcal{P}_{soc})$ and $(\mathcal{P}_{dc})$ are implemented in Python using the Pyomo optimization modeling language [22], [23], using some functions from EGRET [24]. The model is solved using Gurobi [25] to a relative gap of 1%. For the simulations provided, we use a 24-hour recovery horizon with hourly time steps. The simulations were performed on a computer with a 1.9 GHz Intel Core i7 processor with 16 GB of RAM, and the max computation time was 2 hours. The RTS GMLC test system includes renewable generation sources that are must-take, i.e., not curtailable; however, in this work we assume all renewable generation sources are fully curtailable since it is an extreme weather event case study. The resiliency outcomes for this case study are measured by the Expected Unserved Energy (EUE) [26] and the weighted EUE, which we define as:

$$\text{EUE} = \sum_{t\in\mathcal{T}} \sum_{b\in\mathcal{B}} p_{\text{S},b}^t,$$

$$\text{Weighted EUE} = \sum_{t\in\mathcal{T}} \sum_{b\in\mathcal{B}} \beta_b p_{\text{S},b}^t,$$

where the weights $\beta_b \in [0, 1)$ capture the criticality of satisfying the load at bus b, i.e., load shed at buses with greater criticality weight β_b may serve critical infrastructure, such as hospitals and military installments. The weights are arbitrarily assigned once and used for all simulations. We primarily focus on EUE outcomes in this work; however, additional resiliency metrics can be considered [27], [28]. In this work, we assume the investment cost for hardening a line l, generator g, or bus b for the budget constraint in (2) are given by:

1) $C_l = C_l^{\text{base}} + C_l^{\text{mi}} \text{L}_l$ for each line $l \in \mathcal{L}$,
2) $C_g = C_g^{\text{base}} + C_g^{\text{MW}} \overline{P}_g$ for each generator $g \in \mathcal{G}$,
3) $C_b = C_b^{\text{base}} + C_b^{\text{gen}} |\mathcal{G}_b| + C_b^{\text{D}} |\mathcal{D}_b|$ for each bus $b \in \mathcal{B}$,

where C^{base} is the base cost for investing in each component. For line investments, C_l^{mi} is the additional cost to invest in the line per mile and L_l is the length of line l (miles). For generator investments, C_g^{MW} is the additional cost to harden a generator per MW of generation capacity $\overline{P}_g$. For buses, C_b^{gen} is the additional cost per generator located at a given bus, C_b^{D} is the additional cost per load, and $|\mathcal{D}_b|$ is the number of loads that bus b serves. The investment cost parameters used in this case study are given in Table I . These costs are intended to capture the relative costs of hardening these components for model validation, and authors do not claim these costs are accurate.

TABLE I
Investment Cost Parameters

Component	Base Cost ($1000s of USD)	Additional Cost ($1000s of USD)
Lines	$C_l^{\text{base}} = 20$	$C_l^{\text{mi}} = 20$
Generators	$C_g^{\text{base}} = 25$	$C_g^{\text{MW}} = 0.5$
Buses	$C_b^{\text{base}} = 25$	$C_b^{\text{gen}} = 50$ $C_b^{\text{D}} = 25$

A. Hurricane Scenario Generation

We generate synthetic hurricane-like scenarios to demonstrate the proposed resiliency investment framework. For each scenario we make the following assumptions: all wind sources are off due to high winds; other renewable sources (PV and Hydro) impacted at time t remain off for the rest of the recovery horizon; non-impacted photovoltaic (PV) sources in the impacted area and neighboring areas are capturing 20% and 50% of the expected clear-day forecast, respectively; and generators impacted at some time t remain off for the rest of the recovery horizon since the mean time to repair an outage in the RTS GMLC test system is always greater than the 24-hour recovery horizon. We provide a sensitivity study in Section III-E to demonstrate the impact of PV generation on our resiliency model. To generate each weather event scenario s, we:

(1) Initialize hurricane path with respect to the center of the storm (a sequence of buses over the network topology).
(2) Initialize the probability for a component being impacted by the storm each time t as the storm approaches, reaches, and moves away from a component.
    (1) Components that are adjacent to components directly on the hurricane path have lower probabilities of being impacted.
(3) Determine impacted components at each time t in the hurricane scenario.
    (1) If a bus is impacted at time t, the generation sources at that bus are also impacted at time t.
4) Determine recovery time for impacted components. Once a component is impacted, it remains impacted until restored.
    1) Impacted buses will be restored in 8-12 hours after first time t it is impacted.
    2) Impacted lines will be restored in 9-14 hours after first time t it is impacted.

Thus, our multi-period synthetic hurricane scenarios capture grid components being impacted (removed from service) and restored throughout the time horizon. The synthetic hurricane scenarios we use to validate our resiliency investment model can be modified to include fragility models for grid components during extreme weather events, as proposed in [29]. In this case study, we consider three different scenarios, which are illustrated in Fig. 1. Two scenarios are focused in Area 3 of the RTS GMLC test system with varying severity, and one scenario is in Area 2. For the generated scenarios in this work, the vector of probabilities in Step 2

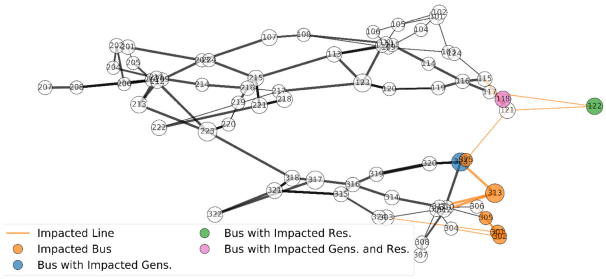

(a) Hurricane Scenario 1. Impacted components: 12 conventional generators, 19 lines, 5 buses, 23 renewable sources. Total cost to harden impacted components: $14.59M USD.

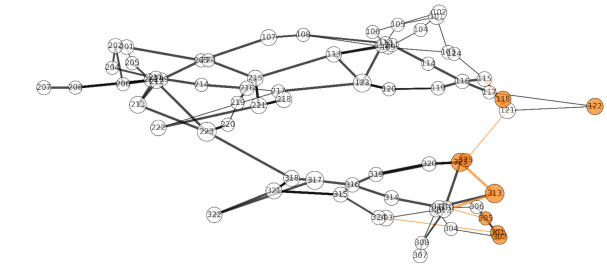

(b) Hurricane Scenario 2. Impacted components: 12 conventional generators, 13 lines, 8 buses, 32 renewable sources. Total cost to harden impacted components: $10.185M USD.

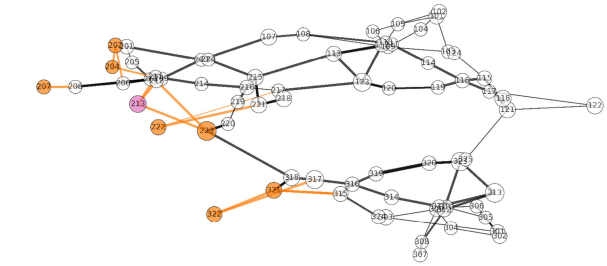

(c) Hurricane Scenario 3. Impacted components: 18 conventional generators, 17 lines, 7 buses, 11 renewable sources. Total cost to harden impacted components: $17.0235M USD.

Fig. 1. Hurricane scenarios generated for this case study. The length of the lines correspond to the line length (in miles) and the larger node sizes correspond to the generation capacity at each bus in RTS GMLC test system. Note that all generation (conventional and renewable) at an impacted bus is also impacted. This is differentiated from buses that are not themselves impacted, but are the location of impacted generation.

is $[0.05, 0.1, 0.15, 0.175, 0.2, 0.175, 0.15, 0.1, 0.05]$, where the increasing then decreasing probability represents the hurricane approaching, reaching, and moving away from each component along the hurricane path.

B. Optimal Transmission Switching for Resiliency

OTS is included in both $(\mathcal{P}_{dc})$ and $(\mathcal{P}_{soc})$ formulations in order to aid the initial impact and recovery during a hurricane scenario. Although known to be computationally difficult, OTS is a way to manage congestion in the network quickly, making it appealing in a resiliency setting. To justify including OTS in our resiliency model, we provide a case study where the resiliency outcome is compared when OTS is enabled and when OTS is disabled. When OTS is enabled, the OTS decision variable $x_l^t \in \{0, 1\}$ is implemented as written in both $(\mathcal{P}_{dc})$ and $(\mathcal{P}_{soc})$. Conversely, when OTS is disabled, the OTS variable is fixed at

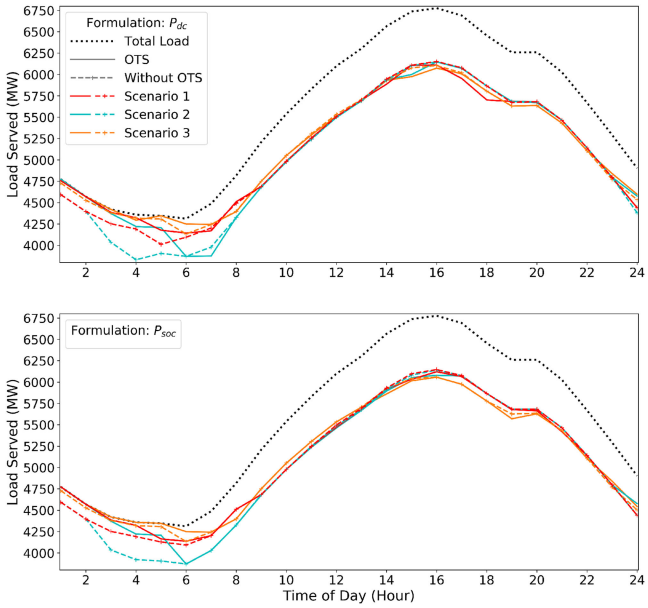

Fig. 2. Comparison of load served and recovery with and without OTS for each scenario when investments are not considered. (top): OTS results for $(\mathcal{P}_{dc})$. Solid lines represent when OTS is enabled and dashed lines represent with OTS is not enabled. (bottom): OTS results for $(\mathcal{P}_{soc})$.

TABLE II
WEIGHTED LOAD SHED (MW) WITH AND WITHOUT OPTIMAL TRANSMISSION SWITCHING (OTS) ENABLED

Experiment	Scenario 1	Scenario 2	Scenario 3
$(\mathcal{P}_{dc})$ no OTS	5537.375	6487.187	5412.361
$(\mathcal{P}_{dc})$ with OTS	5276.829	5766.025	5202.518
$(\mathcal{P}_{soc})$ no OTS	5574.437	6485.955	5444.992
$(\mathcal{P}_{soc})$ with OTS	5330.883	5763.811	5229.024

$x_l^t = 0$ for impacted lines until they recover, and is fixed to 1 otherwise. The impact of including OTS is shown in Fig. 2 for each scenario for the baseline case without any investments, i.e., where $K = \$0$ USD. From Fig. 2, it is seen that OTS has a large impact on mitigating the initial impact of each hurricane scenario in both $(\mathcal{P}_{dc})$ and $(\mathcal{P}_{soc})$ resiliency formulations. Additionally, OTS shows improved recovery at the last few time steps in the recovery horizon for each scenario. Furthermore, including OTS in our resiliency model significantly improves the overall EUE, as shown in Table II. Thus, including an OTS model is an important component of our resiliency investment optimization model.

C. Load Shed Versus Investment Cost Trade-Off

Next, we present a Pareto frontier study to determine the budgets, i.e., the value of K in (2), we will consider for the case studies in the following section. We aim to show the trade-offs between the total cost of optimal investment decisions (generators, lines, and buses) and weighted load shed outcome. Thus, we provide results on the trade-off in optimal investment decisions when a multi-objective optimization problem is considered, i.e., the objective function has a term for both weighted load shed

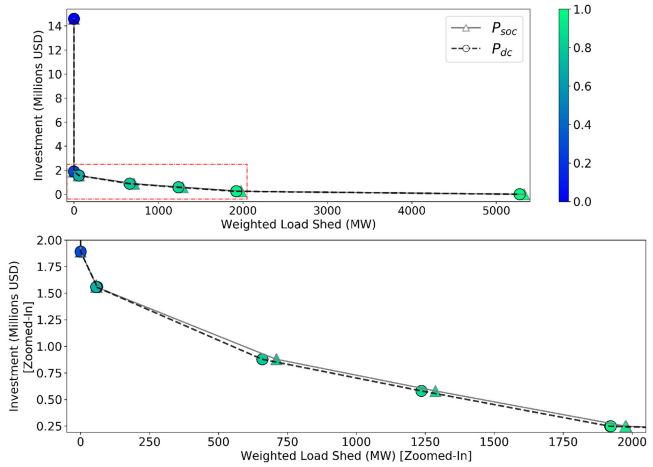

Fig. 3. Pareto frontier for Scenario 1. (top): Pareto frontier for both $(\mathcal{P}_{soc})$ and $(\mathcal{P}_{dc})$ where the blue-green color gradient corresponds to values of $\alpha \in [0.1]$. (bottom): Zoomed in portion of top figure in red box to show the corner of the Pareto frontier.

and the investment cost, which is given by:

$$f_{\text{obj}} = \alpha \frac{1}{A_{\text{IC}}} C_{\text{tot}} + (1-\alpha) \frac{1}{A_{\text{SHED}}} \sum_{t \in \mathcal{T}} \sum_{b \in \mathcal{B}} \beta_b p^t_{\text{S},b}, \quad (44)$$

where $\alpha \in [0,1]$ is the weight of each term in f_{obj}, A_{IC} is the total cost to fix all impacted components, $C_{\text{tot}} = \sum_{b \in \mathcal{B}} C_b z_b + \sum_{g \in \mathcal{G}} C_g z_g + \sum_{l \in \mathcal{L}} C_l z_l$, and A_{SHED} is the weighted total load shed without any resiliency investments. For this study, we solve $(\mathcal{P}_{soc})$ and $(\mathcal{P}_{dc})$ with the objective function f_{obj} in (44) with the budget constraint in (2) omitted. We solve this for various values of α to obtain a convex envelope of the Pareto frontier [30]. For this work, the Pareto frontier demonstrates the trade-off between minimizing the weighted load shed and the total investment cost as $\alpha \in [0,1]$ is varied from 0 to 1. The focus of our simulation results in the following section is to show that investment decisions change as the budget K is varied; thus, the Pareto frontier highlights which total investment amounts will have the greatest impacts on weighted load shed. Furthermore, the Pareto frontier also shows which investment amounts result in diminishing returns on load shed outcomes.

The Pareto frontier for Scenario 1 is shown in Fig. 3. We can see that an investment cost between \$0.25 million and \$2 million USD results in the largest changes in the weighted load shed. We obtain similar results for Scenarios 2 and 3, but they are omitted here due to space constraints. Thus, for the following case studies, we provide resiliency investment results for budget amounts K between \$0.5 million and \$1.25 million USD.

D. Optimal Investment Results

In this section we compare optimal investment results for a \$0.5 million, \$0.75 million, \$1 million, and \$1.25 million USD investment budget, K, for $(\mathcal{P}_{soc})$ and $(\mathcal{P}_{dc})$ for the three hurricane scenarios shown in Fig. 1. For each hurricane scenario, we provide results on the multi-time period recovery over the recovery horizon to illustrate how the investment budget K is spent as the budget varies, and show the EUE and weighted EUE for each budget.

Restoration results, optimal investment decisions, and EUE results are shown for Scenarios 1-3 in Figs. 4-6, respectively. The results for Scenario 1 in Fig. 4(a) demonstrate that the DC approximation power flow model in $(\mathcal{P}_{dc})$ and the SOCP relaxation of the AC power flow model result in different initial impact and recovery results. In particular, for $(\mathcal{P}_{dc})$ the load served is often over-estimated. In Scenario 1, Figs. 4(b)–4(c) highlight how the budget is spent and the differences in investment decisions as the model, i.e., $(\mathcal{P}_{soc})$ vs. $(\mathcal{P}_{dc})$, and budget vary. In Fig. 4(b), with budget $K \geq$\$1 million USD, some of the budget is spent on lines for $(\mathcal{P}_{soc})$ when the AC relaxation is used, whereas none of the budget is spent on lines with the model $(\mathcal{P}_{dc})$ is used. In Scenario 1, from Fig. 4(b) we also see that, for a fixed budget, the amount of the budget spent varies between $(\mathcal{P}_{soc})$ and $(\mathcal{P}_{dc})$. In Fig. 4(c), the investment decisions are compared across both models and various investment budgets. In Fig. 4(c), nodes on the left side represent the set of grid components chosen to investment in at least once for the model variations shown on the right side (either $(\mathcal{P}_{soc})$ or $(\mathcal{P}_{dc})$ and each budget). Components not included on the left side were not invested in with our model. An edge between two nodes represents that the model corresponding to the right endpoint invests in the component on the left endpoints, where dotted edges correspond to $(\mathcal{P}_{dc})$, solid lines correspond to $(\mathcal{P}_{soc})$, and the edge thickness corresponds to the investment cost of the component on the left side. We see that some components are always chosen to invest in regardless of budget or model, such as `118_CC_1` (a generator at bus 118 in Area 1) and `302` (bus 302 in Area 3). However, investment decisions in the other components shown in Fig. 4(c) vary depending on the model used and the investment budget. For example, when $(\mathcal{P}_{dc})$ is used, `302_CT_3` (a generator at bus 302 in Area 3) is rarely chosen to invest in with a given budget, yet `302_CT_3` is always chosen when $(\mathcal{P}_{soc})$ is used. Given that $(\mathcal{P}_{soc})$ is a tighter relaxation of the AC power flow equations, we expect the investment decisions are better-founded, which we investigate further in an AC feasibility study in Section III-F. Lastly, the EUE results for Scenario 1 in Fig. 4(d) shows the DC approximation in $(\mathcal{P}_{dc})$ under-estimates the load shed, and the EUE value with $(\mathcal{P}_{dc})$ is 11% different with $(\mathcal{P}_{soc})$ across the different budgets.

Next, the optimal investment decisions and resiliency outcomes for Scenario 2 are shown in Fig. 5. Similar to the results seen in Scenario 1, the load served results with $(\mathcal{P}_{dc})$ can over-estimate the load served as shown in Fig. 5(a). Fig. 5(b) shows that the amount of the budget invested in each type of component is similar for both models within a fixed budget amount; however, there are minor differences in the amount of the budget spent. Additionally, line hardening investments are only chosen for the largest investment budget, which is similar to what is seen in Scenario 1. Also, Fig. 5(b) shows that for a budget $K \leq$ \$1 million USD, the budget is mostly spent on buses, which is likely due to the large amount of impacted buses in Scenario 2 compared to Scenario 1 (see Fig. 1). In Fig. 5(c), the investment decisions in particular components are compared for both models and various investment budgets for

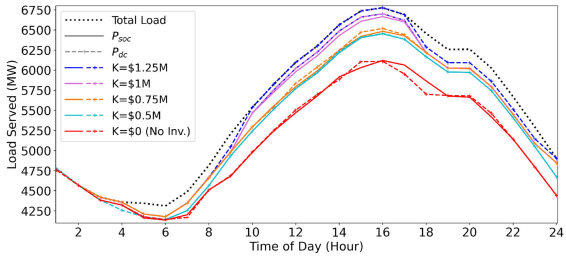

(a) Comparison of the load served and recovery for each budget K. On average over both time and budget, the difference between the load served for the $(\mathcal{P}_{dc})$ and $(\mathcal{P}_{soc})$ models is 0.32% of the total load.

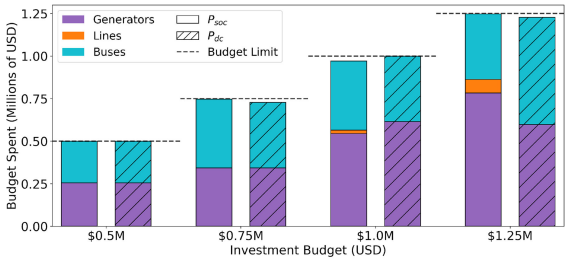

(b) Comparison of investment budget spent as K varies.

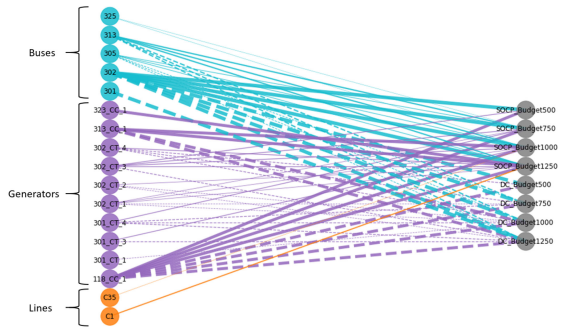

(c) Comparison of investment decisions. Nodes on the left represent grid components, and nodes on the right represent each of the model variations (where the budget is represented in thousands of USD). Edges mean that the model corresponding to the right endpoint invests in the component corresponding to the left endpoint. Dotted edges correspond to $(\mathcal{P}_{dc})$ and solid lines correspond to $(\mathcal{P}_{soc})$. The thickness of the edges is scaled according to the investment cost of the component corresponding to the left endpoint.

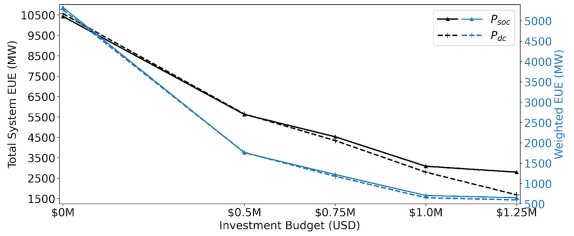

(d) Comparison of EUE and weighted EUE as K varies. On average across the different budgets, the $(\mathcal{P}_{dc})$ value for EUE is 11.0% different than the value from $(\mathcal{P}_{soc})$.

Fig. 4. Comparing $(\mathcal{P}_{soc})$ and $(\mathcal{P}_{dc})$ investment results for Scenario 1. Solid lines and solid-colored regions represent results with $(\mathcal{P}_{soc})$, and dashed lines or hashed regions denote results with $(\mathcal{P}_{dc})$. (a): Comparison of the load served and recovery for each budget K. (b): Comparison of investment decisions as K varies. (c): Comparison of investment choices between $(\mathcal{P}_{soc})$ and $(\mathcal{P}_{dc})$ for each scenario. Nodes on the left represent grid components, and nodes on the right represent each of the model variations. Edges mean that the model corresponding to the right endpoint invests in the component corresponding to the left endpoint. Dotted edges correspond to $(\mathcal{P}_{dc})$ and solid lines correspond to $(\mathcal{P}_{soc})$. The thickness of the edges is scaled according to the investment cost of the component corresponding to the left endpoint. (d): Comparison of EUE and weighted EUE as K varies.

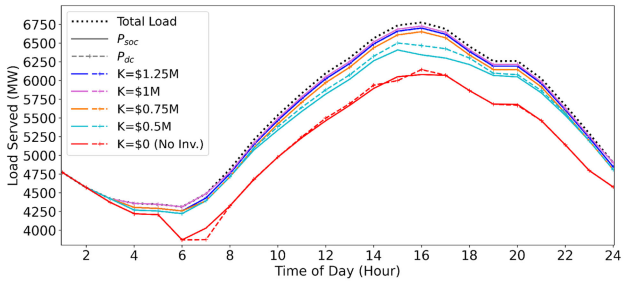

(a) Comparison of the load served and recovery for each budget K. On average over both time and budget, the difference between the load served for the $(\mathcal{P}_{dc})$ and $(\mathcal{P}_{soc})$ models is 0.17% of the total load.

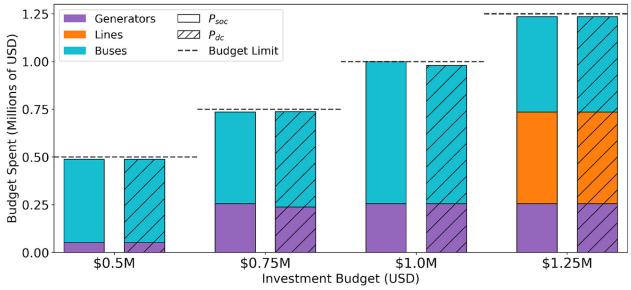

(b) Comparison of investment budget spent as K varies.

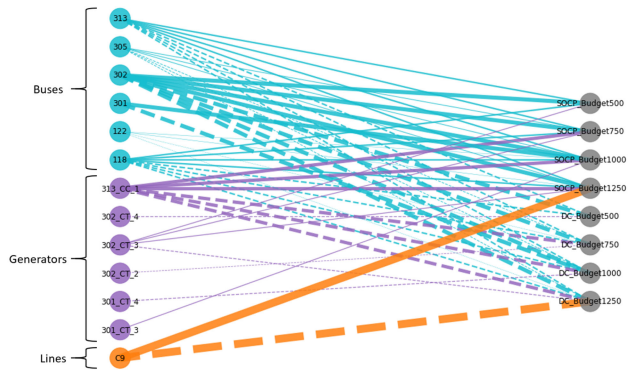

(c) Comparison of investment decisions. Nodes on the left represent grid components, and nodes on the right represent each of the model variations (where the budget is represented in thousands of USD). Edges mean that the model corresponding to the right endpoint invests in the component corresponding to the left endpoint. Dotted edges correspond to $(\mathcal{P}_{dc})$ and solid lines correspond to $(\mathcal{P}_{soc})$. The thickness of the edges is scaled according to the investment cost of the component corresponding to the left endpoint.

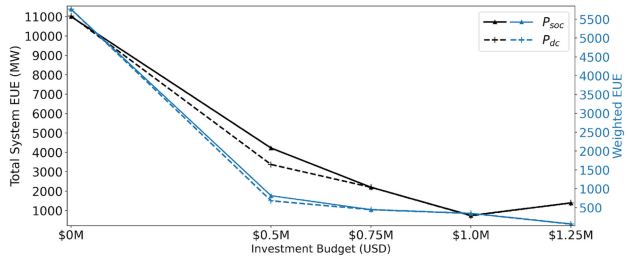

(d) Comparison of EUE and weighted EUE as K varies. On average across the different budgets, the $(\mathcal{P}_{dc})$ value for EUE is 4.4% different than the value from $(\mathcal{P}_{soc})$.

Fig. 5. Comparing $(\mathcal{P}_{soc})$ and $(\mathcal{P}_{dc})$ investment results for Scenario 2. Solid lines and solid-colored regions represent results with $(\mathcal{P}_{soc})$, and dashed lines or hashed regions denote results with $(\mathcal{P}_{dc})$.

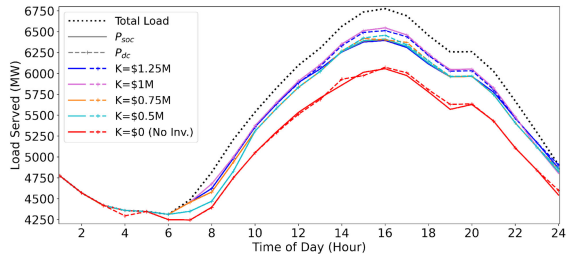

(a) Comparison of the load served and recovery for each budget K. On average over both time and budget, the difference between the load served for the $(\mathcal{P}_{dc})$ and $(\mathcal{P}_{soc})$ models is 0.22% of the total load.

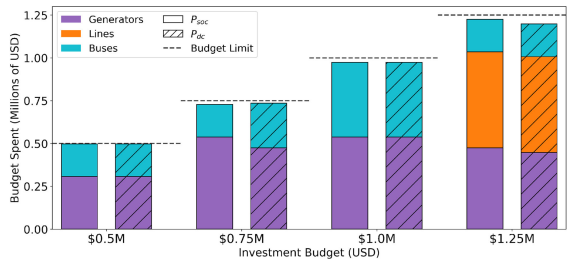

(b) Comparison of investment budget spent as K varies.

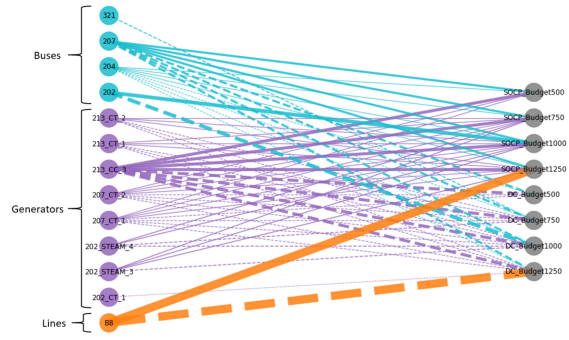

(c) Comparison of investment decisions. Nodes on the left represent grid components, and nodes on the right represent each of the model variations (where the budget is represented in thousands of USD). Edges mean that the model corresponding to the right endpoint invests in the component corresponding to the left endpoint. Dotted edges correspond to $(\mathcal{P}_{dc})$ and solid lines correspond to $(\mathcal{P}_{soc})$. The thickness of the edges is scaled according to the investment cost of the component corresponding to the left endpoint.

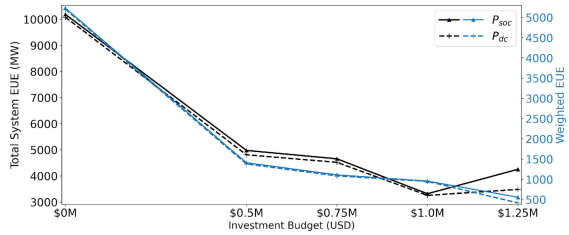

(d) Comparison of EUE and weighted EUE as K varies. On average across the different budgets, the $(\mathcal{P}_{dc})$ value for EUE is 5.5% less than the value from $(\mathcal{P}_{soc})$.

Fig. 6. Comparing $(\mathcal{P}_{soc})$ and $(\mathcal{P}_{dc})$ investment results for Scenario 3. Solid lines and solid-colored regions represent results with $(\mathcal{P}_{soc})$, and dashed lines or hashed regions denote results with $(\mathcal{P}_{dc})$.

Scenario 2. While some optimal investment decisions do not change across various budgets and between the two models, such as buses `313`, `302`, and `118`, we do see that the model used does impact the component chosen in some situations. For example, the generator investment decisions differ depending on whether the $(\mathcal{P}_{soc})$ or $(\mathcal{P}_{dc})$ model is used. In Fig. 5(d) the EUE

TABLE III
EUE RESULTS FOR VARYING LEVELS OF PV GENERATION CAPTURE DURING THE HURRICANE SCENARIO. PV GENERATION OUTPUT X/Y REPRESENTS NON-IMPACTED PV SOURCES IN THE IMPACTED AREA AND NEIGHBORING AREAS ARE CAPTURING X% AND Y% OF THE EXPECTED CLEAR-DAY FORECAST, RESPECTIVELY

Scenario	PV Generation Output	Weighted EUE (MW)	EUE (MW)
1	10/40	732.15	3214.74
1	20/50	707.00	3086.59
1	30/60	683.49	2969.85
2	10/40	346.46	750.44
2	20/50	346.17	744.31
2	30/60	345.67	733.54
3	10/40	952.20	3292.21
3	20/50	956.05	3319.28
3	30/60	958.85	3363.81

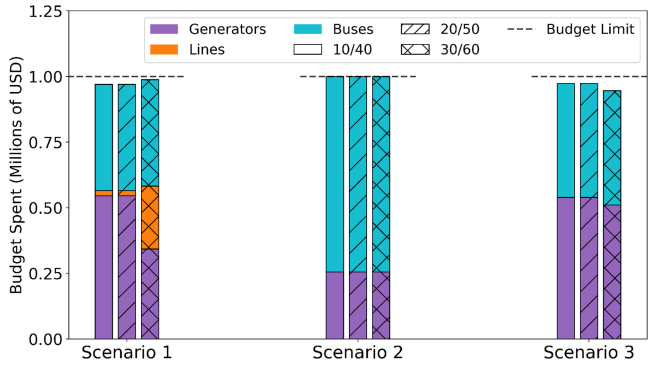

Fig. 7. Comparing investment results as the PV generation output is varied for Scenarios 1, 2, and 3, where the investment budget K =$1.0 M. Let PV generation output X/Y represent non-impacted photovoltaic (PV) sources in the impacted area and neighboring areas are capturing X% and Y% of the expected clear-day forecast, respectively. Solid regions represent results with 10/40, hatched regions represent results with 20/50, and cross-hatched regions represent results with 30/60.

is shown as a function of the investment budget, which illustrates that $(\mathcal{P}_{dc})$ under-estimates the EUE. Interestingly, when the budget K increases from $1 million to $1.25 million USD, the optimal investment decisions that lower the weighted EUE result in an increase in the *unweighted* EUE. This indicates weighting of loads can impact the investment decisions and increase the un-weighted EUE.

Lastly, we show results for Scenario 3 in Fig. 6, which takes place in Area 2 of the network. When comparing the load served and recovery in Fig. 6(a), we again see that the load shed and recovery results vary depending on the network power flow model used. Further, the lower investment budgets result in better recovery at the end of the recovery time horizon, while the larger investment budgets result in increased load served in the middle of the recovery time horizon. In Fig. 6(b), the proportion of the investment budget spend on different components are shown for both models $(\mathcal{P}_{soc})$ and $(\mathcal{P}_{dc})$ and varying investment budget. In Fig. 6(b) we see that line hardening investments are only chosen in Scenario 3 for the largest investment budget, which is a trend also seen in Scenarios 1 and 2. Fig. 6(b) also shows that the budget amount spent can depend on whether the $(\mathcal{P}_{soc})$

TABLE IV
AC FEASIBILITY STUDY RESULTS FOR SCENARIOS 1 AND 3. THE WEIGHTED EUE (W. EUE) AND MAX VIOLATIONS ARE GIVEN IN P.U

Model	Scenario	Budget K (USD)	AC Feas. w. EUE	Resiliency Model w. EUE	Active Power Balance			Reactive Power Balance			Over-voltages	
					Max Violation		Violation	Max Violation		Violation	Max	Violation
					Under	Over	Freq. (%)	Under	Over	Freq. (%)	Violation	Freq. (%)
$(\mathcal{P}_{soc})$	1	\$0.5M	21.194	17.582	0.000	0.099	0.057	0.007	1.342	2.685	0.000	0.000
$(\mathcal{P}_{dc})$	1	\$0.5M	32.971	17.641	0.000	0.179	0.057	0.000	1.672	3.938	0.013	0.342
$(\mathcal{P}_{soc})$	1	\$0.75M	16.990	12.236	0.000	0.675	0.057	0.000	1.348	3.082	0.210	0.285
$(\mathcal{P}_{dc})$	1	\$0.75M	35.746	11.801	0.000	0.000	0.000	0.000	1.348	3.653	0.165	0.457
$(\mathcal{P}_{soc})$	1	\$1.0M	12.012	7.070	0.000	0.211	0.057	0.000	1.350	3.368	0.004	0.057
$(\mathcal{P}_{dc})$	1	\$1.0M	39.939	6.509	0.373	0.000	0.228	0.127	1.350	5.308	0.056	0.742
$(\mathcal{P}_{soc})$	1	\$1.25M	7.746	6.515	0.000	0.000	0.000	0.000	1.350	2.740	0.000	0.000
$(\mathcal{P}_{dc})$	1	\$1.25M	29.225	5.994	0.313	0.498	0.228	0.189	1.350	5.594	0.041	0.457
$(\mathcal{P}_{soc})$	3	\$0.5M	18.471	14.095	0.000	0.00	0.000	0.000	1.348	3.482	0.000	0.000
$(\mathcal{P}_{dc})$	3	\$0.5M	38.577	13.791	0.237	0.041	0.114	0.055	1.346	4.452	0.075	0.685
$(\mathcal{P}_{soc})$	3	\$0.75M	21.583	11.106	0.000	0.382	0.057	0.000	1.348	3.539	0.039	0.171
$(\mathcal{P}_{dc})$	3	\$0.75M	38.712	10.848	0.224	0.000	0.057	0.000	1.700	5.365	0.154	1.142
$(\mathcal{P}_{soc})$	3	\$1.0M	29.656	9.561	0.403	0.000	0.228	0.000	1.699	3.311	0.077	0.685
$(\mathcal{P}_{dc})$	3	\$1.0M	37.082	9.497	0.163	0.000	0.057	0.043	1.505	5.308	0.167	0.913
$(\mathcal{P}_{soc})$	3	\$1.25M	16.216	5.577	0.000	0.000	0.000	0.000	1.504	3.368	0.004	0.057
$(\mathcal{P}_{dc})$	3	\$1.25M	31.633	4.183	0.058	0.000	0.057	0.000	1.699	4.509	0.125	1.084
$(\mathcal{P}_{soc})$	1,2,3 (Avg.)	–	–	–	0.043	0.205	0.057	0.004	1.390	2.397	0.028	0.105
$(\mathcal{P}_{dc})$	1,2,3 (Avg.)	–	–	–	0.183	0.144	0.090	0.058	1.447	3.924	0.076	0.566

or $(\mathcal{P}_{dc})$ model is used. The differences in which specific grid component is invested in is shown in Fig. 6(c). As seen in the previous two scenarios, there are some components that are optimal to harden regardless of whether the $(\mathcal{P}_{soc})$ or $(\mathcal{P}_{dc})$ model is used, such as buses `204` and `207`, and generators `207_CT_2` and `213_CC_3`. However, we see that bus `321` and generator `202_CT_1` are only chosen with the $(\mathcal{P}_{dc})$ model is used, and the $(\mathcal{P}_{soc})$ model determines that the generator `202_STEAM_3` is an optimal investment more often than the $(\mathcal{P}_{dc})$ model. Lastly, the EUE results for Scenario 3 in Fig. 6(d) shows the weighted EUE decreases as the investment budget increases, where the EUE is under-estimated with $(\mathcal{P}_{dc})$ as the budget increases. As in Scenario 2, when the budget is increased from \$1 million to \$1.25 million USD the investment decisions increase the un-weighted EUE while decreasing the weighted EUE, which again shows that weighting the criticality of loads can increase system-wide EUE.

Across all scenarios, our formulation with the DC power flow approximation leads to over-estimating the load served, and can lead to different optimal investment decisions for specific grid components. Additionally, we show that the model's EUE and recovery outcomes differ depending on whether the $(\mathcal{P}_{soc})$ or $(\mathcal{P}_{dc})$ model is used. For all scenarios, mainly generator and bus investments are optimal when the budget is less than \$1 million USD, despite the fact that there are possible line investment options that are less than \$0.5 million USD. When the investment budget is greater than or equal to \$1 million USD, some of the optimal investment decisions include line hardening.

E. PV Generation Sensitivity Study

Next, we demonstrate the impact of PV generation on our resiliency investment model. For this study, the assumed PV generation from non-impacted PV sources in the impacted area and neighboring areas in the network of the expected clear-day forecast is 10% and 40%; 20% and 50%; and 30% and 60%, respectively. The impact of available PV generation on the weighted EUE and EUE is shown in Table III. In Table III, for Scenarios 1 and 2, which are primarily in Area 3 of the network, we see that both weighted EUE and EUE decrease with increased available PV generation, which is due to the large amounts of renewable energy sources in Area 3 in the RTS GMLC test system (relative to both Areas 1 and 2). The difference in sensitivity of the EUE results for Scenario 1 compared to Scenario 2 can also be due to difference in impacted buses and renewable energy sources in these scenarios, since we assume impacted renewable generation cannot be repaired within the optimization horizon and generation at impacted buses are unavailable unless the bus is invested in. In Scenario 3, we do not observe a decrease in weighted EUE or EUE as PV generation increases, which may be due to congestion in the network impacting the ability of renewable generation in Area 3 to be exported to Area 2 during the hurricane scenario. The impact of PV generation on investment decisions, including which grid components to invest in, is shown in Fig. 7. In Scenarios 1 and 3, we see both the investment decisions and the amount of the total investment budget spent changes as PV generation increases. In Scenario 1, we see that as the available PV increases, our resiliency investment model results in fewer generation investments and an increase in line investments. In Scenario 3, as the available PV increases, the investment budget spent decreases due to less investments in generators. We do not observe an impact for Scenario 2, likely due to the large number of impacted renewable energy sources in Scenario 2.

F. AC Feasibility Study

Lastly, an AC feasibility study of the resiliency model results for each scenario is performed to further evaluate the differences in investment decisions, OTS, and generator commitment obtained with $(\mathcal{P}_{soc})$ and $(\mathcal{P}_{dc})$. We solve the non-convex AC power flow (NC-AC) problem to obtain a solution that minimizes

the weighted (according to load criticality parameter β_b) L_2-norm of the difference between NC-AC active power load shed and load shed solution of $(\mathcal{P}_{soc})$ and $(\mathcal{P}_{dc})$, while penalizing over-voltage and power balance violations [31]. We ensure the AC power flow solution satisfies the optimal investment, OTS line status, and generator commitment decisions determined in $(\mathcal{P}_{soc})$ and $(\mathcal{P}_{dc})$ for each budget, as well as the standard power flow line capacity limits and conventional generation dispatch limits. We use Ipopt 3.13.2 [32] to solve the L_2 minimization of the NC-AC problem on the same hardware described above, where an optimal solution was obtained in under 3 minutes for each case study. We initialize the solver at the optimal active power dispatch and load shed, renewable generation curtailment decisions from $(\mathcal{P}_{soc})$ and $(\mathcal{P}_{dc})$, and voltage magnitudes at 1 p.u. The AC feasibility study results are shown in Table IV for Scenarios 1 and 3. In Table IV, the weighted EUE of the AC feasible solution is provided, as well as the weighted EUE of the resiliency model $(\mathcal{P}_{soc})$ or $(\mathcal{P}_{dc})$ for comparison. From Table IV, we show that solutions with locally-minimum violations result in weighted EUE much closer to that obtained with $(\mathcal{P}_{soc})$ than with $(\mathcal{P}_{dc})$. In Table IV, the maximum constraint violations for power balance and over-voltages of all buses in the RTS GMLC system, and the frequency of violations are also provided. The violation frequency is defined as the percent of total instances over all 24 time steps in the recovery horizon and over all 73 buses in the network where there is a power balance or over-voltage constraint violation. We assume violations less than $1\mathrm{e}{-4}$ are treated as 0.0 since the maximum constraint violation parameter in Ipopt is set at $1\mathrm{e}{-4}$. The power balance and over-voltage maximum violations, together with the frequency of these violations, show that we can recover a solution with generally smaller AC power flow constraint violations that happen at a lower frequency with $(\mathcal{P}_{soc})$ compared to $(\mathcal{P}_{dc})$. This is likely due to the $(\mathcal{P}_{dc})$ model's under-estimation of the needed energized lines and dispatchable generators from the OTS and unit commitment decisions, respectively. The authors note the large maximum reactive power balance violations are mainly from buses that are islanded from the network due to investment decisions, yet can satisfy the load located at that bus.

IV. Conclusion

This paper presents a resiliency investment optimization model for determining optimal investments in the transmission grid to protect against extreme weather events using a recovery model based on a second order cone programming (SOCP) relaxation of AC power flow. The investment optimization model determines the optimal investment decisions in the existing transmission grid infrastructure, by considering a recovery model which includes OTS and generator dispatch decisions to minimize unserved load during an extreme weather event. We compare optimal investment decisions obtained when the network is modeled with the SOCP relaxation versus when the network is modeled with the linear DC OPF equations. We provide a case study on the RTS GMLC test system which includes three hurricane scenarios. We demonstrate that including an OTS model in our resiliency investment optimization framework improves the load served during the initial impact of the extreme weather event scenarios, as well as during the restoration phase. The SOCP and DC resiliency investment models result in different investment decisions and their estimates of load served and EUE, where the model with the DC approximation often over-estimates load served. When analyzing the investment decisions, we see that while there are investments common to both the SOCP and DC models, there are differences in some generator and bus investments in each scenario. An AC feasibility study is performed to further evaluate the optimal investment decisions obtained with the SOCP relaxation model versus the DC OPF model, which shows that the SOCP model investment decisions, OTS, and generator dispatch decisions result in fewer locally-minimal over-voltage and power balance violations than the linear DC model. This suggests that the SOCP model is making better-informed decisions than the DC OPF model and is giving a more accurate estimation of load served during the recovery horizon. Lastly, a sensitivity study shows that the type of grid components chosen as optimal investment decisions are impacted by the amount of available PV generation during the extreme weather event scenarios.

Future work includes developing weather scenarios based on historical data and incorporating uncertainty into the current formulation to determine the impact on resiliency outcomes. Future directions also include applying our resiliency investment model on additional networks, and investigating ways to reduce the computation time and improve the scalability of solving $(\mathcal{P}_{soc})$. Incorporating optimal electrical energy storage investment and placement is another approach for promoting resiliency to compare with the current model EUE outcomes, as well as other resiliency metrics.

Acknowledgment

The authors are thankful for productive discussions with Anya Castillo and Manuel J. Garcia about various studies in this paper. The views expressed in the article do not necessarily represent the views of the U.S. Department of Energy or the U.S. Government.

References

[1] *Executive Office of the President* "Benefits of increasing electric grid resilience to weather outages," *President's Council of Economic Advisors and the U.S. Department of Energy's Office of Electricity Delivery and Energy Reliability*, 2013. [Online]. Available: https://www.energy.gov/sites/default/files/2013/08/f2/Grid%20Resiliency%20Report_FINAL.pdf

[2] D. T. Ton and W. P. Wang, "A more resilient grid: The U.S. department of energy joins with stakeholders in an R&D plan," *IEEE Power Energy Mag.*, vol. 13, no. 3, pp. 26–34, May 2015.

[3] Y. Wang, C. Chen, J. Wang, and R. Baldick, "Research on resilience of power systems under natural disasters-a review," *IEEE Tran. Power Syst.*, vol. 31, no. 2, pp. 1604–1613, Mar. 2016.

[4] *Before and After the Storm - Update: A Compilation of Recent Studies, Programs, and Policies Related to Storm Hardening and Resiliency*, Edison Electric Institute, Washington D.C., USA, Accessed: Jun. 29, 2020. [Online]. Available: https://docplayer.net/3644617-Before-and-after-the-storm-a-compilation-of-recent-studies-programs-and-policies-related-to-storm-hardening-and-resiliency-update.html

[5] B. J. Pierre, B. Arguello, A. Staid, and R. T. Guttromson, "Investment optimization to improve power system resilience," in *Proc. IEEE Int. Conf. Probabilistic Methods Appl. Power Syst.*, 2018, pp. 1–6.

[6] B. J. Pierre, B. Arguello, and M. J. Garcia, "Optimal investments to improve resilience considering initial transient response and long-term impacts," in *Proc. IEEE Int. Probabilistic Methods Appl. Power Syst.*, 2020, pp. 1–6.
[7] H. Nagarajan, E. Yamangil, R. Bent, P. Van Hentenryck, and S. Backhaus, "Optimal resilient transmission grid design," in *Proc. Power Syst. Comput. Conf.*, 2016, pp. 1–7.
[8] A. Bagheri, C. Zhao, F. Qiu, and J. Wang, "Resilient transmission hardening planning in a high renewable penetration era," *IEEE Trans. Power Syst.*, vol. 34, no. 2, pp. 873–882, Mar. 2019.
[9] Y. Fang, C. Fang, E. Zio, and M. Xie, "Resilient critical infrastructure planning under disruptions considering recovery scheduling," *IEEE Trans. Eng. Manag.*, vol. 68, no. 2, pp. 452–466, Apr. 2021.
[10] G. Patsakis, I. Aravena, and D. Rajan, "A stochastic program for black start allocation," in *Proc. 52nd Hawaii Int. Conf. Syst. Sci.*, 2019, pp. 3659–3668.
[11] A. Arab, A. Khodaei, S. K. Khator, and Z. Han, "Electric power grid restoration considering disaster economics," *IEEE Access*, vol. 4, pp. 639–649, 2016.
[12] S. Ma, B. Chen, and Z. Wang, "Resilience enhancement strategy for distribution systems under extreme weather events," *IEEE Trans. Smart Grid*, vol. 9, no. 2, pp. 1442–1451, Mar. 2018.
[13] Y. Tan, A. K. Das, P. Arabshahi, and D. S. Kirschen, "Distribution systems hardening against natural disasters," *IEEE Trans. Power Syst.*, vol. 33, no. 6, pp. 6849–6860, Nov. 2018.
[14] W. Yuan, J. Wang, F. Qiu, C. Chen, C. Kang, and B. Zeng, "Robust optimization-based resilient distribution network planning against natural disasters," *IEEE Trans. Smart Grid*, vol. 7, no. 6, pp. 2817–2826, Nov. 2016.
[15] G. Huang, J. Wang, C. Chen, J. Qi, and C. Guo, "Integration of preventive and emergency responses for power grid resilience enhancement," *IEEE Trans. Power Syst.*, vol. 32, no. 6, pp. 4451–4463, Nov. 2017.
[16] P. Dehghanian, S. Aslan, and P. Dehghanian, "Maintaining electric system safety through an enhanced network resilience," *IEEE Trans. Ind. Appl.*, vol. 54, no. 5, pp. 4927–4937, Sep. 2018.
[17] M. Bynum, A. Castillo, J.-P. Watson, and C. D. Laird, "Evaluating demand response opportunities for power systems resilience using MILP and MINLP formulations," *AIChE J.*, vol. 65, no. 7, Jul. 2019, Art. no. e16508.
[18] B. Kocuk, S. S. Dey, and X. A. Sun, "New formulation and strong MISOCP relaxations for AC optimal transmission switching problem," *IEEE Trans. Power Syst.*, vol. 32, no. 6, pp. 4161–4170, Nov. 2017.
[19] C. Coffrin and P. V. Hentenryck, "Transmission system restoration with co-optimization of repairs, load pickups, and generation dispatch," *Int. J. Elect. Power*, vol. 72, pp. 144–154, 2015.
[20] H. Nagarajan, R. Bent, P. V. Hentenryck, S. Backhaus, and E. Yamangil, "Resilient transmission grid design: AC relaxation vs. DC approximation," 2017. [Online]. Available: https://arxiv.org/abs/1703.05893
[21] C. Barrows *et al.*, "The IEEE reliability test system: A proposed 2019 update," *IEEE Trans. Power Syst.*, vol. 35, no. 1, pp. 119–127, Jan. 2020, doi: 10.1109/TPWRS.2019.2925557.
[22] W. E. Hart *et al.*, *Pyomo - Optimization Modeling in Python*. 2nd ed., Berlin, Germany: Springer Science & Business Media, 2017.
[23] W. E. Hart, J.-P. Watson, and D. L. Woodruff, "Pyomo: Modeling and solving mathematical programs in python," *Math. Program. Comput.*, vol. 3, no. 3, pp. 219–260, 2011.
[24] B. Knueven, C. Laird, J.-P. Watson, M. Bynum, A. Castillo, and US-DOE, *Egret V. 0.1 (beta)*. 2019. [Online]. Available: https://www.osti.gov//servlets/purl/1498854
[25] Gurobi Optimization, LLC, "Gurobi optimizer reference manual," 2019. [Online]. Available: http://www.gurobi.com
[26] "Probabilistic adequacy and measures," North American Electric Reliability Corporation (NERC), Atlanta, GA, USA, 2018. Accessed: Jun. 29, 2020. [Online]. Available: https://www.nerc.com/comm/PC/Probabilistic%20Assessment%20Working%20Group%20PAWG%20%20Relat/Probabilistic%20Adequacy%20and%20Measures%20Report.pdf
[27] S. Poudel, A. Dubey, and A. Bose, "Probabilistic quantification of power distribution system operational resilience," in *Proc. IEEE Power Energy Soc. Gen. Meeting*, 2019, pp. 1–5.
[28] E. Vugrin, A. Castillo, and C. Silva-Monroy, "Resilience metrics for the electric power system: A performance-based approach," Sandia National Laboratories, Albuquerque, NM, USA, Tech. Rep. SAND2017-1493, 2017. [Online]. Available: https://www.osti.gov/biblio/1367499
[29] M. Panteli, C. Pickering, S. Wilkinson, R. Dawson, and P. Mancarella, "Power system resilience to extreme weather: Fragility modeling, probabilistic impact assessment, and adaptation measures," *IEEE Trans. Power Syst.*, vol. 32, no. 5, pp. 3747–3757, Sep. 2017.
[30] Y. Cui, Z. Geng, Q. Zhu, and Y. Han, "Review: Multi-objective optimization methods and application in energy saving," *Energy*, vol. 125, pp. 681–704, 2017.
[31] I. Aravena, D. Rajan, G. Patsakis, S. S. Oren, and J. Rios, "A scalable mixed-integer decomposition approach for optimal power system restoration," 2019. [Online]. Available: http://www.optimization-online.org/DB_HTML/2019/02/7062.html
[32] A. Wächter and L. Biegler, "On the implementation of an interior-point filter line-search algorithm for large-scale nonlinear programming," *Math. Prog.*, vol. 106, pp. 25–57, 2006.

Kaitlyn Garifi (Member, IEEE) received the B.S. degree in bioengineering and the B.A. degree in mathematics from the University of California, Santa Cruz, Santa Cruz, CA, USA, in 2015, and the M.S. and Ph.D. degrees in electrical engineering from the University of Colorado Boulder, Boulder, CO, USA, in 2017 and 2020, respectively. Her research interests include stochastic optimization, power grid resiliency, and smart grid technologies.

Emma S. Johnson received the B.A. degree in mathematics from St. Olaf College, Northfield, MN, USA, in 2017. She is currently working toward the Ph.D. degree in operations research with the Georgia Institute of Technology, Atlanta, GA, USA. Since 2015, she has been an Intern with Sandia National Laboratories, Albuquerque, NM, USA. Her research interests include mixed-integer programming, disjunctive programming, and scalable methodology for power systems optimization.

Bryan Arguello (Member, IEEE) received the M.S.E. degree in operations research from the University of Texas at Austin, Austin, TX, USA and the M.A. degree in mathematics from the University of Colorado at Boulder, Boulder, CO, USA. He is currently a Senior Member of Technical Staff with the Operations Research and Computational Analysis Department, Sandia National Laboratories, Albuquerque, NM, USA. His research interests include mixed-integer programming, scheduling, and bilevel programming applied to power systems resilience, microgrid cost analysis, and other national security applications.

Brian J. Pierre (Senior Member, IEEE) received the Ph.D. degree in electrical engineering from Arizona State University focused on electric power systems, Tempe, AZ, USA. He is currently a Principal Member of the Technical Staff with the Electric Power Systems Research Department, Sandia National Laboratories, Albuquerque, NM, USA. His research interests include power system modeling, power system resilience, power system optimization, power system dynamics, and renewable energy integration. He was the recipient of the R&D 100 Award in 2017 and was awarded the 2020 IEEE Albuquerque Section Outstanding Young Engineer Award for the development of algorithms and software tools to co-optimize grid resilience and reliability.